Coupling Hydrophobicity, Dispersion, and Electrostatics in Continuum Solvent Models

J. Dzubiella,* J. M. J. Swanson, and J. A. McCammon

NSF Center for Theoretical Biological Physics (CTBP), and Department of Chemistry and Biochemistry, University of California, San Diego, La Jolla, California 92093-0365, USA

(Received 13 September 2005; published 3 March 2006)

An implicit solvent model is presented that couples hydrophobic, dispersion, and electrostatic solvation energies by minimizing the system Gibbs free energy with respect to the solvent volume exclusion function. The solvent accessible surface is the output of the theory. The method is illustrated with the solvation of simple solutes on different length scales and captures the sensitivity of hydration to the particular form of the solute-solvent interactions in agreement with recent computer simulations.

DOI: 10.1103/PhysRevLett.96.087802 PACS numbers: 61.20.−p, 68.03.−g, 82.60.Lf, 87.15.−v

Much progress has been made in the last decade in the understanding of hydrophobic solvation on different length scales [1,2]. Most of this work has been devoted to study solvation of purely repulsive, hard-sphere-like solutes, while less attention has been given to the influence and incorporation of dispersion or electrostatic contributions. Likewise, an entire field in the biophysical community has explored electrostatic solvation effects in the absence or uncoupled addition to hydrophobic considerations; see, e.g., [3] for a review. Recently, however, several computer simulations have demonstrated a strong coupling between hydrophobicity, solute-solvent dispersion attractions, and electrostatics. For example, simulations of explicit water between platelike solutes revealed that hydrophobic attraction and dewetting phenomena are strongly sensitive to the nature of solute-solvent dispersion interactions [4,5]. Similarly, simulations of hydrophobic channels [6,7] and nanosolutes [8] have shown that electrostatic potentials strongly affect the dewetting behavior and potentials of mean force (pmf). A fully atomistic simulation of the folding of the two-domain protein BphC enzyme [9] further supported coupling by showing that the region between the two domains was completely dewetted when solvent-solute van der Waals (vdW) and electrostatic interactions were turned off, but accommodated 30% of the density of bulk water with the addition of vdW attractions, and 85%–90% with the addition of electrostatics, in accord with experimental results. Finally, Liu *et al.* recently observed a dewetting transition in the collapse of the melittin tetramer, which was strongly sensitive to the type and location of the hydrophobic residues proving that these observations apply to realistic biomolecular systems [10].

In this Letter we propose a continuum description of solvation that explicitly couples hydrophobic, dispersion, and electrostatic contributions. We express the Gibbs free energy as a *functional* of the solute cavity shape, the latter given by the volume exclusion function of the solvent [11], and obtain the optimal shape by minimization. This leads to an expression similar to the Laplace-Young equation for the geometrical description of capillary surfaces [12], but in contrast to existing approaches *explicitly* includes the inhomogeneous distributions of dispersion and electrostatic contributions as well as curvature corrections. Geometry-based approaches similar to our formalism exist in related fields, such as the Helfrich description of membranes shapes [12], wetting in colloids and granular media [12], and electrowetting [13]. We stress that, as opposed to other implicit solvent models, the solvent accessible surface (SAS) is an output of our theory. We begin by verifying that our method is able to describe the solvation of small alkanes on molecular scales. We then demonstrate that it captures the strong sensitivity of dewetting and hydrophobic hydration to solute-solvent interactions on larger scales for a model system of two alkane-assembled spheres. In this striking example the strong hydrophobic attraction decreases almost 2 orders of magnitude in units of the thermal energy, k_BT, and dewetting is partially or completely suppressed when realistic dispersion and electrostatic contributions are included. We expect our approach to be particularly useful in solvation studies of proteins, where the hydrophobic surfaces are highly irregular and laced with hydrophilic units [1,10] and superhydrophobic nanosolutes [15].

Let us consider an assembly of solutes with arbitrary shape and composition surrounded by a dielectric solvent in a macroscopic volume $\mathcal{W}$. We define a subvolume $\mathcal{V}$ empty of solvent for which we can assign a volume exclusion function in space given by $v(\vec{r}) = 0$ for $\vec{r} \in \mathcal{V}$ and $v(\vec{r}) = 1$ elsewhere. We assume that the surface bounding the volume is continuous and closed. The absolute volume V and interface area S of $\mathcal{V}$ can then be expressed as functionals of $v(\vec{r})$ via $V[v] = \int_{\mathcal{W}} d^3r[1 - v(\vec{r})]$ and $S[v] = \int_{\mathcal{W}} d^3r|\vec{\nabla} v(\vec{r})|$, where $\vec{\nabla} \equiv \vec{\nabla}_{\vec{r}}$ is the usual gradient operator. The density distribution of the solvent is either zero or ρ_0 defined by $\rho(\vec{r}) = \rho_0 v(\vec{r})$, where ρ_0 is the bulk density of the solvent at fixed temperature and pressure. The solutes' positions and conformations are fixed.

We suggest expressing the Gibbs free energy $G[v]$ of the system as a functional of $v(\vec{r})$ and obtaining the optimal volume and surface via minimization $\delta G[v]/\delta v(\vec{r}) = 0$. We adopt the following ansatz for the Gibbs free energy:

$$G[v] = PV[v] + \int_{\mathcal{W}} d^3r\gamma(\vec{r})|\vec{\nabla}v(\vec{r})| + \int_{\mathcal{W}} d^3r\rho(\vec{r})U(\vec{r}) + \frac{\epsilon_0}{2}\int_{\mathcal{W}} d^3r\{\vec{\nabla}\Psi(\vec{r})\}^2\epsilon(\vec{r}). \quad (1)$$

The first term in (1) is the energy of creating a cavity in the solvent against the difference in bulk pressure between the liquid and vapor, $P = P_l - P_v$. The second term describes the energetic cost due to solvent rearrangement close to the cavity surface in terms of a parameter $\gamma(\vec{r})$. This interfacial energy penalty is thought to be the main driving force for hydrophobic phenomena [1]. $\gamma(\vec{r})$ is not only a solvent specific quantity but also depends on the topology of the surface in a nonlocal way [16]; i.e., it is a functional of the volume exclusion function, $\gamma(\vec{r}) = \gamma(r;[v])$. The exact form of this functional is not known. For planar macroscopic solvent-cavity interfaces $\gamma(\vec{r})$ is usually identified by the liquid-vapor surface tension, γ_{lv}, of the solvent, which we also employ here. Furthermore, we make a *local curvature approximation;* i.e., we assume that $\gamma(\vec{r})$ can be expressed solely as a function of the local mean curvature of the cavity interface, $\gamma(\vec{r}) = \gamma(H(\vec{r}))$, with $H(\vec{r}) = [\kappa_1(\vec{r}) + \kappa_2(\vec{r})]/2$, where κ_1 and κ_2 are the two principal curvatures. We then apply the first order curvature correction to γ_{lv} given by scaled-particle theory [17], the commonly used ansatz to study the solvation of hard spheres, arriving at

$$\gamma(\vec{r}) = \gamma_{\mathrm{lv}}[1 - 2\delta H(\vec{r})], \quad (2)$$

where δ is a constant and positive length expected to be of the order of the solvent particle size [17]. The curvature is positive or negative for convex or concave surfaces, respectively. Note that this leads to an increased surface tension for concave surfaces. It has been shown by simulations that (2) predicts the interfacial energy of growing a spherical cavity in water rather well for radii $\gtrsim 3$ Å [18].

The third term in (1) is the total energy of the nonelectrostatic solute-solvent interaction given a density distribution $\rho_0 v(\vec{r})$. The energy $U(\vec{r}) = \sum_i U_i(\vec{r} - \vec{r}_i)$ is the sum of the short-ranged repulsive and long-ranged attractive dispersion interactions U_i between each solute atom i and a solvent molecule. Classical solvation studies typically represent U_i as an isotropic Lennard-Jones (LJ) potential, $U_{\mathrm{LJ}}(r) = 4\epsilon[(\sigma/r)^{12} - (\sigma/r)^6]$, with an energy scale ϵ and a length scale σ. The importance of treating dispersion interactions independently, as opposed to absorbing them into the surface tension term, has been emphasized by Gallicchio *et al.* in their study of cyclic alkanes [19].

The fourth term in (1) describes the total energy of the electrostatic field expressed by the local electrostatic potential $\Psi(\vec{r})$ and the position-dependent dielectric constant $\epsilon(\vec{r})$ assuming linear response of the dielectric solvent. The electrostatic potential Ψ is evaluated by Poisson's equation, $\vec{\nabla}\cdot[\epsilon(\vec{r})\vec{\nabla}\Psi(\vec{r})] = -\lambda(\vec{r})/\epsilon_0$, where $\lambda(\vec{r})$ is the solute's charge density distribution. The most common approximation for $\epsilon(\vec{r})$ is proportional to the volume exclusion function $v(\vec{r})$ [3]

$$\epsilon(\vec{r}) = \epsilon_v + v(\vec{r})(\epsilon_l - \epsilon_v), \quad (3)$$

where ϵ_v and ϵ_l are the dielectric constants inside and outside the volume $\mathcal{V}$, respectively.

Plugging in (2) and (3) in functional (1) and using the calculus of functional derivatives, the minimization yields

$$0 = P + 2\gamma_{\mathrm{lv}}[H(\vec{r}) - \delta K(\vec{r})] - \rho_0 U(\vec{r}) - \frac{\epsilon_0}{2}[\vec{\nabla}\Psi(\vec{r})\epsilon(\vec{r})]^2\left(\frac{1}{\epsilon_l} - \frac{1}{\epsilon_v}\right). \quad (4)$$

Equation (4) is a partial second order differential equation for the optimal solvent accessible volume and surface expressed in terms of pressure, surface curvatures, dispersion interactions, and electrostatics, all of which have dimensions of force per surface area or energy density. $K(\vec{r}) = \kappa_1(\vec{r})\kappa_2(\vec{r})$ is the Gaussian curvature and follows from the variation of the surface integral over $H(\vec{r})$ in (1). Thus, in our approach the geometry of the surface, expressed by H and K, is directly related to the inhomogeneous dispersion and electrostatic energy contributions. Note that the SAS is presently defined with respect to the LJ centers of the solvent molecules.

In the following we illustrate solutions of (4) in spherical and cylindrical symmetries. For a spherical solute (4) reduces to a function of R, the radius of the solvent accessible sphere, $H = 1/R$ and $K = 1/R^2$. In cylindrical symmetry the SAS can be expressed by a one-dimensional shape function $r(z)$, where z is the coordinate on the symmetry axis and r the radial distance to it. The surface in three-dimensional space is obtained by revolving $r(z)$ around the z axis. The principal curvatures are then given by $\kappa_1 = -1/(r\sqrt{r'^2 + 1})$ and $\kappa_2 = r''/[(r'^2 + 1)^{3/2}]$, where the primes indicate the partial derivative with respect to z. We solve (4) and Poisson's equation numerically, using standard forward time relaxation schemes.

We now study the solvation of methane and ethane in water and compare our results to the simple point charge (SPC) explicit water simulations by Ashbaugh *et al.* [20], in which the alkanes are modeled by neutral LJ spheres [21]. We fix the liquid-vapor surface tension for SPC water at 300 K to $\gamma_{\mathrm{lv}} = 65$ mJ/m^2 [18]. Since we deal with water under ambient conditions, the pressure term can be neglected and the length δ remains the only free parameter. For methane we can reproduce the simulation solvation energy ΔG with a fit $\delta = 0.85$ Å. This is in good agreement with Huang *et al.* [18] who measured $\delta = 0.76 \pm 0.05$ Å for SPC water. Solving the cylindrically symmetric problem for the diatomic ethane with the same $\delta = 0.85$ Å, we obtain a fit-parameter-free $\Delta G = 11.40$ kJ/mol, which is only 7% larger than the simulation results. Alternatively, the best fit $\delta = 0.87$ Å reproduces the simulation energy exactly. This is surprisingly good agreement given the crude curvature correction we apply and the fact

that the large curvature of the system varies locally in space. This supports the validity of our continuum approach down to a molecular scale. The curvature and shape functions $H(z)$, $K(z)$, and $r(z)$ are plotted in Fig. 1 together with the vdW surface and the canonical SAS obtained from rolling a probe sphere with a typically chosen radius $r_p = 1.4$ Å over the vdW surface [14]. Away from the center of mass $|z| \gtrsim 1$ Å the curvatures follow the expected trends $H \simeq 1/R$ and $K \simeq 1/R^2$ with $R \simeq 3.1$ Å for the spherical surfaces. The surface resulting from our theory is smaller than the canonical SAS, and is smooth at the center of mass ($z = 0$) where the canonical SAS has a kink. Thus, our surface has a smaller mean curvature at $z = 0$ and an almost zero Gaussian curvature, which is typical for a cylinder geometry for which one of the principal curvatures is zero. These results may justify the use of smooth surfaces in coarse-grained models of closely packed hydrocarbon surfaces, a possibility we now explore with solvation on larger length scales where dewetting effects can occur.

Let us consider two spherical solutes that we assume to be homogeneously assembled of CH_2 groups with a uniform density $\rho = 0.024$ Å^{-3} up to a radius $R_0 = 15$ Å, defined by the maximal distance between a CH_2 center and the center of the solute [22]. The integration of the CH_2-water LJ interaction over the volume of a sphere yields a 9-3-like potential for the interaction between the center of the paraffin sphere and a water molecule [23]. The intrinsic, nonelectrostatic solute-solute interaction $U_{ss}(r_{12})$ in a center-to-center distance r_{12} can be obtained in a similar fashion. The solvation of the two solutes is studied for a fixed surface-to-surface distance, which we define as $s_0 = r_{12} - 2R_0$. We obtain an effective SAS radius of one sphere of about $R \simeq R_0 + 2.4$ Å so that the effective surface-to-surface distance is roughly $s \simeq s_0 - 4.8$ Å. Since we are also interested in the effects of charging up the solutes we place opposite charges $\pm Ze$, where e is the elementary charge, in the center or on the edge of the two spheres.

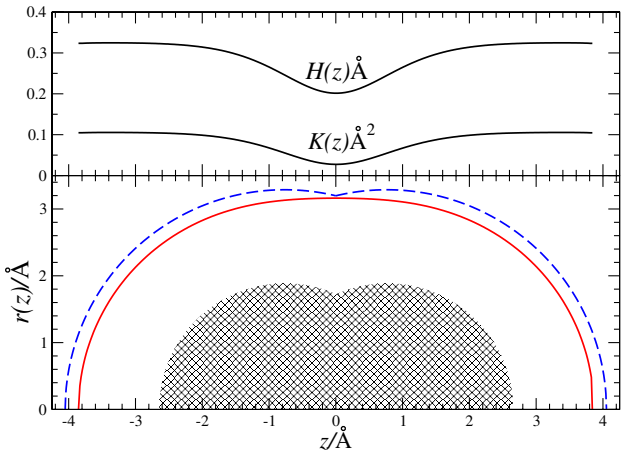

FIG. 1 (color online). Mean $H(z)$ and Gaussian $K(z)$ curvature and shape function $r(z)$ (solid lines) for ethane. The canonical SAS (dashed line) from rolling a probe sphere with radius $r_p = 1.4$ Å over the vdW surface (shaded region) is also shown.

In the following we focus on a separation distance of $s_0 = 8$ Å to investigate the influence of different contributions to the energy functional on the shape function, $r(z)$, and the curvatures, $K(z)$ and $H(z)$. For $s_0 = 8$ Å, it follows that $s \simeq 3.2$ Å, such that two water molecules could fit between the solutes on the z axis. We systematically change the solute-solute and solute-solvent interactions, as summarized in Table I. We begin with only the LJ repulsive interactions in system I and then add a curvature correction with $\delta = 0.75$ Å, vdW attractions, and sphere-centered charges $Z = 4$ and $Z = 5$ in systems II–V, respectively. To study the influence of charge location, we reduce the magnitude of each charge in system VI to $Z = 1$ and move them to the edge of the spheres on the symmetry axis such that they are 8 Å apart (indicated by arrows in Fig. 2). The surface tension and dielectric constant of the vapor and liquid are fixed to $\gamma_{lv} = 72$ mJ/m^2, $\epsilon_v = 1$, and $\epsilon_l = 78$, respectively.

The results for the curvatures and $r(z)$ for systems I–VI are shown in Fig. 2. Away from the center of mass ($|z| \gtrsim 10$ Å), systems I–VI show very little difference. The curvatures are $H \simeq 1/R$ and $K \simeq 1/R^2$ with $R \simeq 17.4$ Å. Close to the center of mass ($z \simeq 0$), however, the influence of changing the parameters is considerable. In system I, Eq. (4) reduces to the minimum surface equation $H(z) = 0$ for $z \simeq 0$. For two adjacent spheres the solution of this equation is the catenoid $r(z) \propto \cosh(z)$, which features zero mean curvature (κ_1 and κ_2 cancel each other) and negative Gaussian curvature. This leads to a vapor bubble bridging the solutes. When curvature correction is applied (system II), the mean curvature becomes nonzero and negative (concave) at $z \simeq 0$, while the Gaussian curvature grows slightly more negative. As a consequence, the total enveloping surface area becomes larger and the solvent inaccessible volume shrinks; i.e., the value of $r(z \simeq 0)$ decreases. Turning on solute-solvent dispersion attraction amplifies this trend significantly as demonstrated by system III. Mean and Gaussian curvatures increase fivefold, showing strongly enhanced concavity, and the volume empty of water decreases considerably, expressed

TABLE I. Studied systems for two alkane-assembled spherical solutes. If $r(z = 0) \neq 0$ the system is "dewetted." In VI the solutes' charge is located off-center (OC) at the solute surface.

System	δ (Å)	vdW attraction	Z	$W(s_0)/k_BT$	Dewetted
I	0.00	no	0	−57.6	yes
II	0.75	no	0	−34.1	yes
III	0.75	yes	0	−6.3	yes
IV	0.75	yes	4	−9.2	yes
V	0.75	yes	5	−5.1	no
VI	0.75	yes	1 (OC)	−1.3	no

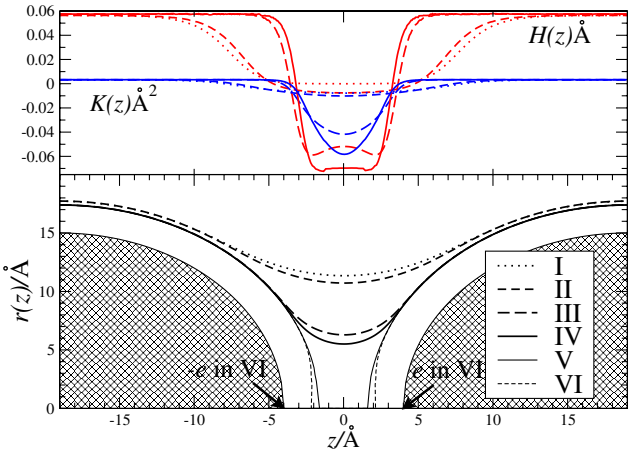

FIG. 2 (color online). Mean $H(z)$ and Gaussian $K(z)$ curvatures and shape function $r(z)$ for two alkane-assembled solutes of radius $R_0 = 15$ Å (shaded region) for systems I–VI. The position of the charges $Z = \pm 1$ in VI are indicated by arrows. Curvatures are not shown for the "wet" systems V and VI.

by $r(z = 0) \simeq 10.7$ Å dropping to $r(z = 0) \simeq 6.3$ Å. These trends continue with the addition of electrostatics in system IV. When the sphere charges are further increased from $Z = 4$ to $Z = 5$ (system IV $\rightarrow$ V), we observe a wetting transition: the bubble ruptures and the SAS jumps to the solution for two isolated solutes, where $r(z \simeq 0) = 0$. The same holds when going from III to VI, when only one charge, $Z = 1$, is placed at each of the solutes' surfaces. Importantly, this demonstrates that the present formalism captures the sensitivity of dewetting phenomena to specific solvent-solute interactions as demonstrated in previous studies [4–10]. Note that the SAS at $|z| \simeq 2$ Å is closer to the solutes in VI compared to V due to the proximity of the charge to the interface. Clearly, the observed effects, in particular, the transition from III to VI, cannot be described by existing solvation models, which use the SAS [14], or effective surface tensions and macroscopic contact angles [12] as input.

The significant change of the SAS with the solute-solvent interaction has a strong impact on the pmf, $W(s_0) = G(s_0) - G(\infty) + U_{ss}(s_0)$. Values of $W(s_0 = 8$ Å) are given in Table I. From system I to VI the total attraction between the solutes decreases almost 2 orders of magnitude. Interestingly, the curvature correction (I $\rightarrow$ II) lowers W by a large $23.5 k_B T$, even though $R \gg \delta$. A striking effect occurs when vdW contributions are introduced (II $\rightarrow$ III): the intersolute attraction decreases by $\simeq 28 k_B T$ while the dispersion solute-solute potential, $U_{ss}(s_0 = 8$ Å), changes by only $-0.44 k_B T$. Similarly, adding charges of $Z = 5$ (III $\rightarrow$ V) at the solutes' centers or $Z = 1$ (III $\rightarrow$ VI) at the solutes' surfaces decreases the total attraction by $1.2 k_B T$ and $5 k_B T$, respectively. Note that the total attraction decreases although electrostatic attraction has been added between the solutes. The same trends have been observed in explicit water simulations of a similar system of charged hydrophobic nanosolutes [8].

These results clearly demonstrate that solvation effects and solvent mediated phenomena are not only strongly influenced by solute-solvent interactions, but that these interactions are inherently coupled. By including coupling, our formalism captures the balance between hydrophobic, dispersive, and electrostatic forces, which has been observed in previous studies [4–10] but never described in a single theoretical framework. Nonpolar and polar coupling is expected to be crucial for a complete characterization of biomolecular solvation. The present formalism is limited only by the crude curvature and dielectric descriptions currently employed. Future efforts to improve these approximations are critical to accurately describe solvation effects on multiple length scales and for more complicated geometries.

The authors thank Tushar Jain, John Mongan, and Cameron Mura for useful discussions. J. D. acknowledges financial support from a DFG Forschungsstipendium. The work in the McCammon group is supported by NSF, NIH, HHMI, CTBP, NBCR, and Accelrys, Inc.

*Electronic address:jdzubiella@ucsd.edu

[1] D. Chandler, Nature (London) **437**, 640 (2005).
[2] G. Hummer *et al.*, Chem. Phys. **258**, 349 (2000).
[3] B. Roux and T. Simonson, Biophys. Chem. **78**, 1 (1999).
[4] X. Huang *et al.*, J. Phys. Chem. B **109**, 3546 (2005).
[5] N. Choudhury and B. M. Pettitt, J. Am. Chem. Soc. **127**, 3556 (2005).
[6] J. Dzubiella and J.-P. Hansen, J. Chem. Phys. **120**, 5001 (2004).
[7] S. Vaitheesvaran *et al.*, J. Chem. Phys. **121**, 7955 (2004).
[8] J. Dzubiella and J.-P. Hansen, J. Chem. Phys. **119**, 12 049 (2003).
[9] R. Zhou *et al.*, Science **305**, 1605 (2004).
[10] P. Liu *et al.*, Nature (London) **437**, 159 (2005).
[11] D. Beglov and B. Roux, J. Chem. Phys. **104**, 8678 (1996).
[12] P. Kralchevsky and K. Nagayama, *Particles at Fluid Interfaces and Membranes* (Elsevier, Amsterdam, 2001).
[13] T. Chou, Phys. Rev. Lett. **87**, 106101 (2001).
[14] M. L. Connolly, J. Mol. Graphics **11**, 139 (1993).
[15] K. K. S. Lau *et al.*, Nano Lett. **3**, 1701 (2003).
[16] D. G. Triezenberg and R. Zwanzig, Phys. Rev. Lett. **28**, 1183 (1972).
[17] F. H. Stillinger, J. Solution Chem. **2**, 141 (1973).
[18] D. M. Huang *et al.*, J. Phys. Chem. B **105**, 6704 (2001).
[19] E. Gallicchio *et al.*, J. Phys. Chem. B **104**, 6271 (2000).
[20] H. S. Ashbaugh *et al.*, Biophys. J. **75**, 755 (1998).
[21] The LJ water-atom parameters are $\epsilon = 0.8941$ kJ/mol and $\sigma = 3.45$ Å for CH_4, and $\epsilon = 0.7503$ kJ/mol and $\sigma = 3.47$ Å for CH_3, and the bond length of ethane is 1.53 Å.
[22] The CH_2-water LJ parameters are $\epsilon = 0.5665$ kJ/mol and $\sigma = 3.536$ Å. Similar ones have been used by Huang *et al.* [4] to study dewetting between paraffin plates.
[23] D. M. Huang and D. Chandler, J. Phys. Chem. B **106**, 2047 (2002).